## *Microtechnology Department*

Head: C. Dücső

Research and development of physical, chemical/biochemical sensors and integrated systems:

- MEMS and MEMS related technology, with special emphasis on development of Si MOS embedding circuits.
- Development and applications of near IR light emitting diodes and detectors.
- Solar cells and their competitive technology.
- Acoustic wave devices and their application.

Fundamental research on:

- sensing principles
- novel materials and nanostructures
- novel 3D fabrication techniques
- ion-solid interaction for supporting MEMS development.

Device and material characterisation

### MEMS

*Head:*
Dr. C. Dücső, Ph.D.

*Staff:*
György Altmann, technician
Mária Ádám, M.Sc., res. fellow
Prof. Dr. István Bársony, D.Sc.
Dr. Ferenc Beleznay, D.Sc.
Ábel Debreczeny, B.Sc.
Magdolna Erős, technician
Csilla Faragó, technician
János Ferencz, M.Sc., engineer
Dr. Péter Fürjes, Ph.D.
Alajos Gondos, technician
†Dr. Béla Keszei, dr. univ., res. fellow
Ákos Majoros, M.Sc., engineer
Attila Nagy, technician
Margit Pajer, technician
Dr. Imre Szabó, dr. univ., engineer
Éva Vázsonyi, M.Sc., res. fellow
János Volk Ph.D. applicant, res. Fellow

*Visiting Research Scientist:*
L. Fedák (University of Uzhgorod, Guest of the House of Professors and MFA)

### Optoelectronic Devices

*Head:*
Dr. B. Szentpáli, Ph.D.

*Staff:*
Dr. Olga Krafcsik Homokiné Ph.D. mothercraft
Dr. Zoltán Lábadi, Ph.D.
Dr. Ákos Nemcsics Ph.D. habil. part time 30%
Dr. István Pintér Ph.D.
Dr. Bálint Pődör Ph.D.., part time 30%
Dr. Sándor Püspöki engineer, dr. univ.
Dr. Vilmos Rakovics Ph.D.
István Réti engineer
Varga Ferencné technician
Ms. Katalin Vörös Veresné engineer

*PhD Students (Advisor):*
Edvárd Bálint Kuthi (István Pintér)
Ágoston NémethH (Zoltán Lábadi)

*Engineering trainee:*
László Klagyivik

### Semiconductor Characterisation

*Head:*
Dr. G. Battistig, Ph.D.

*Staff:*
Edvard Badaljan
Dr. László Dózsa Ph.D.
Dr. Zoltán Hajnal Ph.D.
Dr. Zsolt J. Horváth Ph.D.
Tibor Mohácsy
Dr. Nguyen Q. Khánh Ph.D.
Zsuzsa Püspöki
András Ster
József Waizinger

*Visiting Research Scientist:*
Yolanda Morilla, (Centro Nacional de Aceleradores, Sevilla, Spain. TéT Spanish-Hungarian bilateral cooperation)

*Ph.D. Students (Advisor):*
Péter Basa (Dr. Zsolt J. Horváth)
Anita Pongrácz (Dr. Gábor Battistig)

## MEMS Laboratory (C. Dücső)

### *Sensor Array for Fast Explosion-Proof Gas Monitoring "SAFEGAS" (EU-FP5 2000-2003, accepted in 2004)*

M. Ádám, I. Bársony, C. Dücső, P. Fürjes, É. Vázsonyi

A Si based four element integrated calorimetric sensor was developed and constructed for olfactory detection of hydrocarbon mixtures up to their Lower Explosion Limit (LEL) concentration. The integrated sensor array chip consists of three pellistors and one heat conductivity sensor. In order to construct a four-wire, inherently explosion-proof transmitter, the power consumption of each sensor was reduced below 50mW and a sequential read-out scheme was adopted.

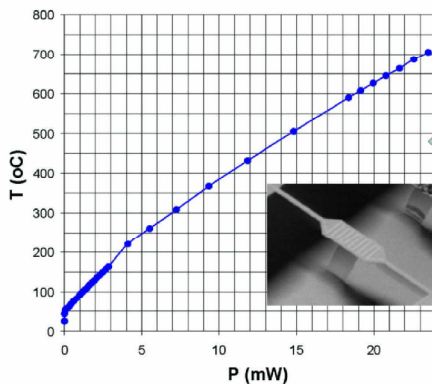


*Fig.1: Power dissipation of the 100x100μm$^2$ microhotplate developed at MFA*

The role of MFA was the development of the sensor array chip. We have elaborated a novel technology based on porous Si micromachining for the formation of low power consumption microhotplates (Fig.1), which are the basic elements in both sensors. We applied dip & drop technique was for coating the hotplate's surface with Pt-catalysts and reference materials in the pellistors (Fig.2). The reference heater of the heat conductivity sensor was encapsulated by Si cap (Fig.3). Due to the reduced power dissipation of the sensor elements the driver and read-out electronics of the transmitter became inherently explosion-proof. Consequently, only the sensor chip must be explosion protected because of the high surface temperature of the calorimetric sensors.

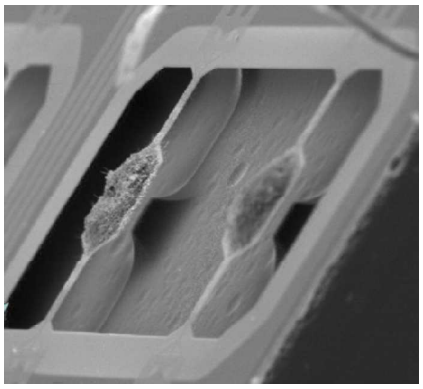

*Fig.2: SEM view of a pellistor. Catalyst coated hotplate (left), the passive reference pair coated by pure $Al_2O_3$ (right)*

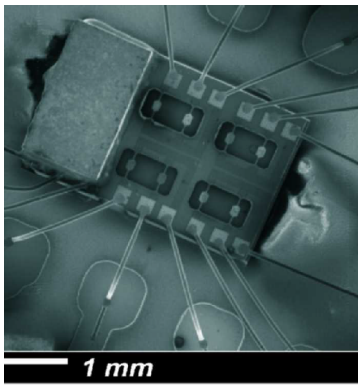


*Fig.3: The sensor array chip consists of 3 pellistors and one heat conductivity sensor. Its reference element is encapsulated by a Si cap (left)*

Olfactory detection is based on the method proposed by ALPHAMOS Co., France uses principal component analysis (PCA) and partial least square (PLS) fitting. The system developed by WESZTA-T Ltd., Hungary is capable to distinguish and measure methane, propane, butane and hexane mixtures.

## *Sensing Computers and Telepresence "TeleSense" (NKFP 032/2001)*

M. Ádám, I. Bársony, C. Dücső, P. Fürjes, É. Vázsonyi

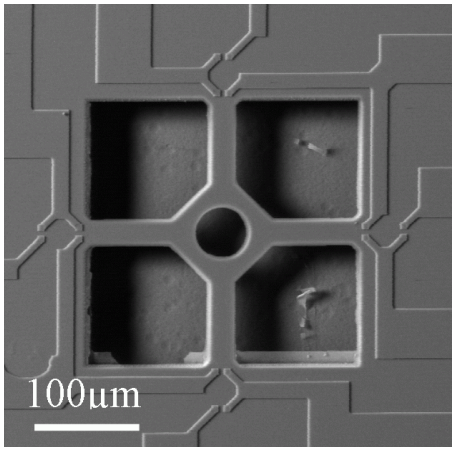


*Fig.1: Scanning electron micrograph of the sensor structure. Characteristic dimensions: bridge 80x32x10 µm$^3$, plate 100x100x10 µm$^3$, hole 50 µm diameter, cavity depth cc. 35 µm.*

One of the major goals of this project was the development of an integrable micro-force sensor capable of resolving the three vector components of the loading force. An array of this element will be used for tactile sensing.

We have successfully adopted the porous Si micromachining technique for the fabrication of single crystalline force sensor elements. Four piezoresistors were formed in an n-type perforated membrane, having their reference pairs on the substrate in order to detect the mechanical stress by four half-bridges. We successfully combined the HF based porous Si process with conventional doping and Al metallisation, thereby offering the possibility of integration with readout and amplifying electronics. The 300x300 µm$^2$ membrane (Fig.1) size allows the formation of large area arrays for tactile sensing using single crystalline deforming elements of superior mechanical properties.

Although the bare structure meets the requirements set for force detection (Fig.2), a protective, flexible coating on top is essential for any real application. Therefore, we have started systematic investigation of the effects of various coverages on sensitivity and lateral resolution.

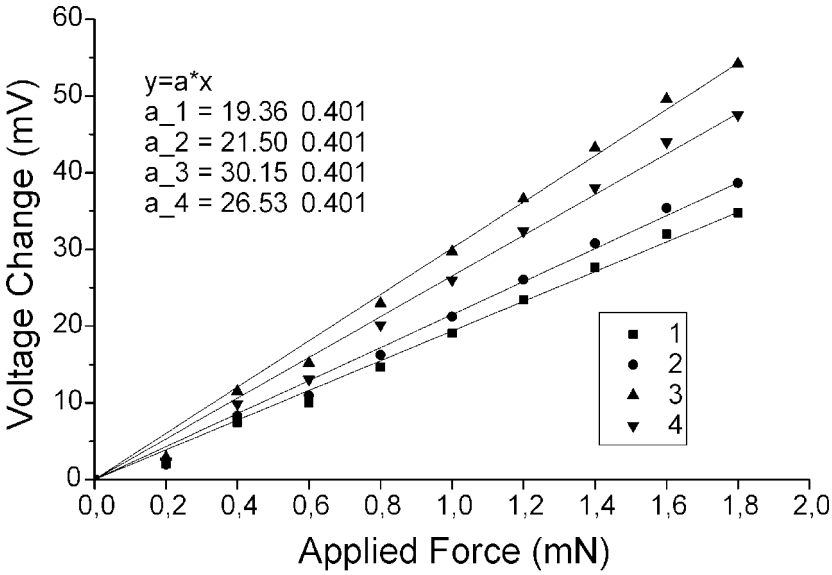


*Fig.2: Linear responses of the four piezoresistive bridges of one sensing element for normal load. The difference in the slopes is the result of the non central positioning of the loading tip on the small area membrane. The sensitivity is 4-6 mV/mN/V*

## *Ceramic Substrates for SAW Devices, "CERSAW" (NATO SfP)*

F. Beleznay, J. Ferencz

The main objective of the project was to realise piezoceramic substrates as an alternative to single-crystals for SAW applications. The aim is to get cheaper, at-request and reliable substrates suitable for large-scale production.
Our task was to develop device technology and suitable filter structures to qualify piezoelectric substrates for SAW applications. We have adopted our SAW filters processing technology for the present material technology, developed at Köporc and TKI, Budapest, and made model filters on larger (40 mm diameter) wafers. Having fixed basic SAW parameters on these elements, we have designed special filter structures to separate and investigate degrading second order effects, such as diffraction, large dielectric permeability, spurious bulk waves, internal reflections between transducer and the electromagnetic leakage in the substrate. Since electromagnetic leakage dominating we have designed a "symmetric double-output" filter structure, where the outputs are shifted by half wavelength from each other, and in this way difference of the two output signals sums up the acoustic signals but subtracts the electromagnetic ones. Figures 1.a-c show characteristics of these filters made on standard $LiNbO_3$ substrates and on the investigated ceramic substrates, respectively.

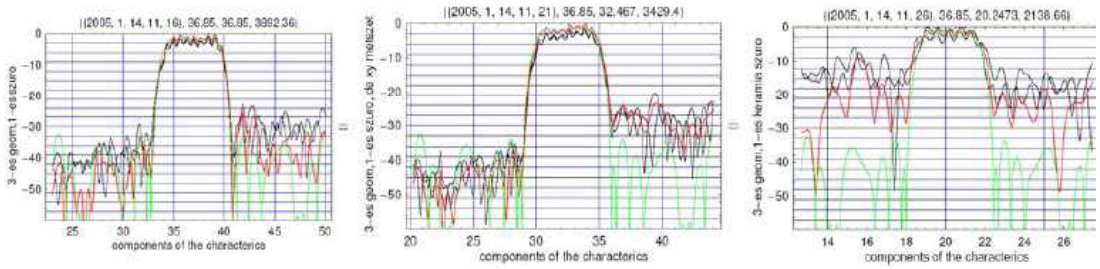


*Fig.1a-c: Transfer characteristics of an "apodized symmetric double-output" filter on 128$^o$ cut $LiNbO_3$, XY cut $LiNbO_3$, and a ceramic filter. Two traditional outputs (black), the measured analog difference of these outputs (red) and the theoretical (green) characteristics are shown.*

Each of the characteristics shows diffraction effects, which are due to the finite length of the individual electrode pairs, and are partly suppressed on the anisotropic crystalline $LiNbO_3$ surfaces. In isotropic ceramic materials diffraction can not be suppressed, hence characteristics are much less structured; this is seen in the band stop region next to the band pass one. Another characteristic is the spurious bulk wave. In general, bulk wave is also generated and detected by the interdigital transducers; this generation in crystalline material depends on the orientation of the surface and on the propagation direction. The 128$^o$ cut $LiNbO_3$ is best known where bulk wave gene-ration is minimal (a), on the other hand XY cut $LiNbO_3$ has spurious bulk wave, velocity of this is about 15% faster than the surface wave, as is seen on the higher frequency side of the pass-band. Ceramic filter has a much higher spurious at the high energy side.
Ceramic materials have inherent drawbacks such as **unavoidable diffraction, bulk waves generation and significant dielectric constant**. These all together makes most probable that they may have applications only in new fields, such as resonator struc-

tures, and/or composite layered structures. Application of **thin layers and confined (waveguide mode) surface wave may solve most of the problems** we have detected.

### *Porous Si Multilayers for Optical Devices*

I. Bársony, J. Volk

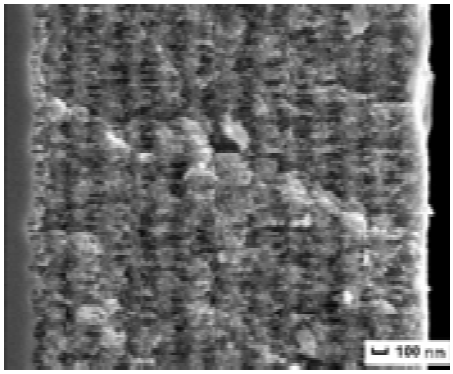


*Fig.1: Fabry-Perot filter by 27 a element porous Si multilayer*

Controlled formation of porous Si multilayers was elaborated in order to form optical elements, e.g. Bragg-reflectors, Fabry-Perot filters (Fig.1). The refractive index of the porous Si layer can be tuned by the porosity (the volume ratio of void and Si in the layer) i.e. by varying current density during the electrochemical etching process. The main advantage of the high/low optical density multilayered structure lies in its transferability for liquids and gases, therefore their application for sensing chemical or biochemical materials is feasible.
Ellipsometric and reflectometric investigations of the multilayer structures show, that simple periodic variation of current density doesn't result in reproducible porosity in the corresponding layers. In order to investigate this effect we have constructed a dedicated system for measuring the reflectance spectra ($\lambda$=400-1100nm) of the multilayer during the formation process. The 1s sampling rate enables us to monitor the dynamic change of the optical properties in the forming multilayers. In a detailed analysis and comparison with optical model calculations we concluded that parallel with the electrochemical process at the porous-Si/Si front a continuous photochemical dissolution of the previously formed porous Si layers results in their lower optical density. This phenomenon effects on the optical parameters of the structure, e.g. results in a blue-shift of the resonant peak in a Fabry-Perot filter (Fig.2). The in-situ reflectance spectrum analysis may provide appropriate data for on-line controlling of porous Si multilayer formation.

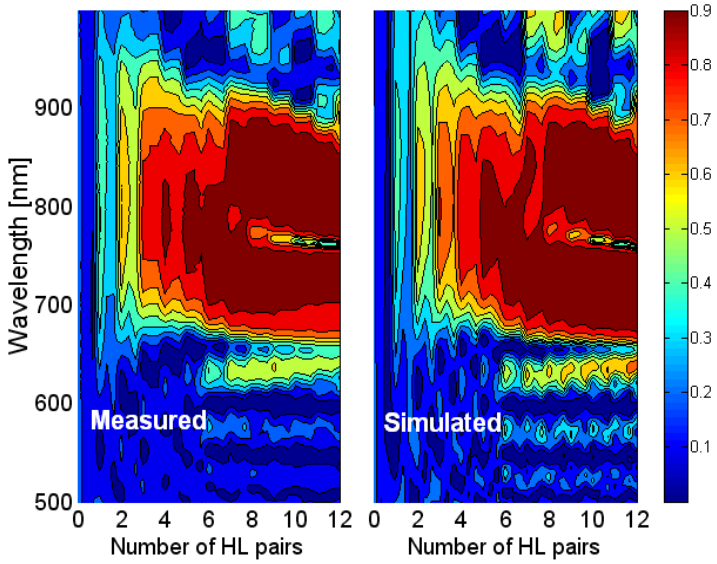


*Fig.2: Blue-shift of the resonant peak in a Fabry-Perot filter by increasing the number of the high/low optical density pairs (denoted by H and L), i.e. the etching time. The resonant peak is present after the formation of the LL resonator ($8^{th}$ HL pairs).*

## Laboratory of Optoelectronic Devices (B. Szentpáli)

### *Solar Cell Innovation Centre (NKFP 3/025/2001 )*

**Z. Lábadi,** Á. Németh, S. Püspöki; V. Rakovics, I. Réti, A. Tóth, Ms. Varga Ferencné, Ms. K. Vörös Veresné

***Aim and achievements:***

The overall aim of the project is to develop a thin film preparation system for R&D on solar cells with CuInGaSe active layer. MTA MFA conducts applied research in this project as a participant in a consortium.

In the frame of this overall scheme a magnetron sputtering module was installed by the KRAFT Rt and tested by the researchers of the institute.

The main technical features of the equipment include 30x30cm substrate size, DC and pulse mode electric supply, three target places for rectangular shaped targets and a software control facility.

Deposition of contact layers for CIGS solar cells

The purpose of this work is to develop an optimal technology for the deposition of transparent front contact layer for a CIGS solar cell. The structure consists of an undoped ZnO buffer layer and an Al doped conductive ZnO (ZAO) layer. The magnetron sputtering of the ZAO layer takes place from a Zn:Al (2%m/m) metallic target in Ar:$O_2$ atmosphere. Mechanical movement, gas pressure and composition, DC electric supply and additional pulse parameters are fully computer controlled.

The figure shows the construction of the solar cell.

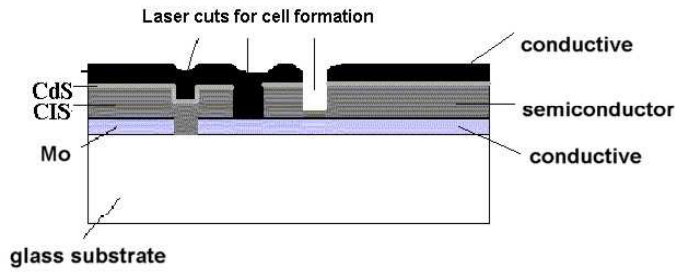


*Construction scheme of a CIGS solar cell*

Use of ceramic ZnO targets determines the parameters of the deposited film leaving little room for parameter optimalisation. Furthermore these targets are relatively expensive and the deposition rate is largely limited by the allowed thermal dissipation of the target. Our reactive sputtering method offers an alternative against deposition from ceramic targets and a possibility of scale-up the technology. A further advantage is that the transparency and conductivity of the layer can be controlled in wide range of parameters by technological means.

The layers are qualified by spectral transparency, sheet resistance, SEM microscopy and XPS spectroscopy. Our experiments show that the pulse parameters, sputter power density and the gas composition are the critical parameters for finding the optimum between conductivity and transparency.

ZnO depositions for possible sensor applicationsIt was also shown that by appropriate setting of the sputtering parameters a non-stochiometric porous ZnO layer can be deposited (referred as por-ZnO below).

Layers were deposited in the 2-20 micron thickness range. All of those layers were non-transparent by visual inspection. They were subsequently characterised by SEM microscopy, Electron Dispersive Spectrum (EDS), ellipsometry, and four point probe sheet resitance.

SEM morphology of a typical por-ZnO layer exhibits 50 nm average crystallite size with uniform porosity. Semi-quantitative EDS examination shows substantial lack of oxygen compared to the stoichiometric material. Specific resistance of the material is in the 1E-2 Ohmcm range.
Due to the non-stoichiometric composition, nanoscale crystallite size and porous character of the layer this material seems to be a promising candidate for gas sensor applications.

CdS/InP model system for understanding CdS/CIGS interface
In thin film polycrystalline Cu(In,Ga)Se2/CdS/ZnO solar cells, the active CIGS/CdS interface plays a main role to further improvements of their performance. This interface is complex and its formation is under active investigation. We have undertaken a specific study of the interface indium chemical modifications during CdS growth using single crystalline InP wafers and CdS obtained by chemical bath deposition (CBD), as a reference system for the case of the CIGS/CdS interface. We have investigated the behaviour of the thin layer formed on the InP surface during the first minutes of the growth of the CdS layer on (100) oriented p-InP wafer. The composition of the interface is analyzed before by means of XRD. XRD rocking curve contains strong sharp peaks of $\beta$-$In_2S_3$. CdS/InP interface also contains small amount of Cd(OH)2 or CdSO3. These results are relevant to several aspects of to the CIGS/CdS interfaces as shown by parallel experiments.
$\beta$-$In_2S_3$ can replace CdS buffer layer, improving the environmental safety of the CIGS solar cell technology. We could prepare high quality $\beta$-$In_2S_3$ layers by successive evaporation of the elements.

## *ADVOKATE – Advanced Dry Process for Low Cost Thin Multicrystalline Silicon Solar Cell Technology (EU-FP6: ENK6-CT-2001-00562, 2001-2004)*

**I. Pintér,** J. Ferencz, B. Forgács, G. Dóra, Á. Majoros, É. Vázsonyi, E. Kuthi, Ms. Payer Károlyné, A. Gondos, C. Faragó

***Aim and achievements***:
Within the project our task was the R&D of Plasma Immersion Ion Implantation (PIII) technology.
The PIII technique is a very low energy (100-1000eV) implantation.
At MFA the PIII technique have been used for Phosphorous doping of the emitter of Silicon solar cells.
The advantage of the PIII are:

- very fast process (5-60s)
- good reproducibility and homogeneity of the dose
- can be integrated into dry solar cell processing technology

A vacuum chamber was constructed in which 4 pieces 10x10 $cm^2$ multicrystalline silicon wafers can be processed together. The system is also capable PIII processing of two 12.5x12.5$cm^2$ wafers or a single 15x15$cm^2$ wafer. The sheet resistance of the emitters can be adjusted in 25-300 Ohm/sq range, so it can be applied for either selective or homogeneous emitter cells.

Metallisation of solar cells are performed by two basic technologies:
a/ Lift-off technique of evaporated Ti/Pd/Ag layers
b/ screen printing of silver and Aluminium pastes (under development)

***Results:***
First not optimised selective emitters prepared by PIII resulted in **12.2-13.55%** cell's efficiencies on multicrystalline silicon.
Internal quantum efficiencies of the PIII cells prepared from Polix mc-Si from different batches showed similar and very good blue sensitivity.

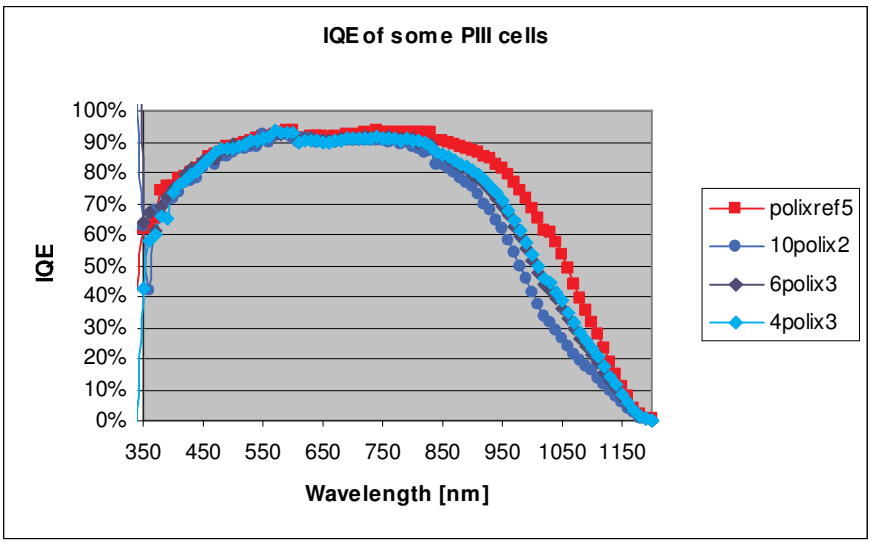


### *The origin of electronic noise in semiconductor sensors (OTKA T 037706)*

**B. Szentpáli,** V. Rakovics, T. Mohácsy, I. Bársony, I. Réti, Ms. M. Ádám Antalné, L. Klavigyik

***Aim and achievements:***
The lower limit of the sensitivity of any sensor is limited by the noise, fluctuation generated in them. The magnitude of this noise determines the dynamic range of the sensor too. Namely the maximum of the perceptible signal, which results in a proportional output signal, is also limited. This limitation follows from the working principle of the sensor [154]. The pressure-, temperature-, gas-sensors work in low frequency range from a few hundred Hz down to mHz. The output of sensors of high frequency signals (microwave, optical) is usually a filtered, averaged resulting in a slowly varying voltage. Therefore the noise of sensors in the low frequency range - from a few Hz to 100 kHz - has a great importance.
In 2004 two investigations were performed:
1. The noise in porous Si structures. As it is well known originally the porous Si was intend to apply for light emitting diode. These efforts have had no real success. Nowadays the porous Si is applied in micromachining technique for fabricating different sensors. In this respect the electric conduction mechanisms and the fluctuations in this material have importance. The current-voltage characteristics and the low-frequency noise spectra of p-type Si - Porous Si - Al diode like structures were investigated [151]. Over 1 V forward biases a reasonable fit was obtained in the Fowler-Nordheim plot. Any attempts of accurately fitting the I-V characteristic by other known transport mechanisms failed. At lower biases, however, an additional current-component appears which shows a saturating character. This current component is ascribed to trap-assisted tunnelling. The measured noise spectra show 1/f character; however the magnitude of the noise shows saturation with increasing biases instead of the usual case, where the noise power scales with $I^2$, or $V^2$. This finding is interpreted by a model of two parallel current paths. The noise arising from the smaller and saturating current determines the noise performance of the whole device.

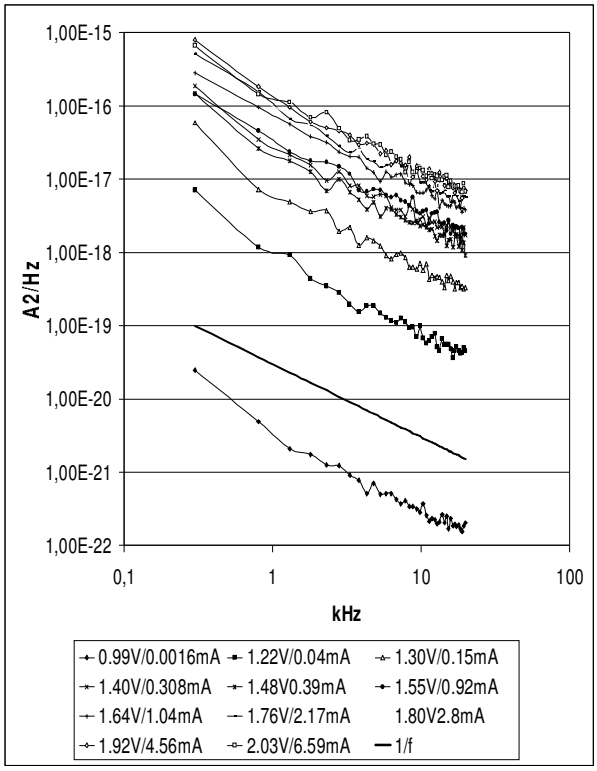


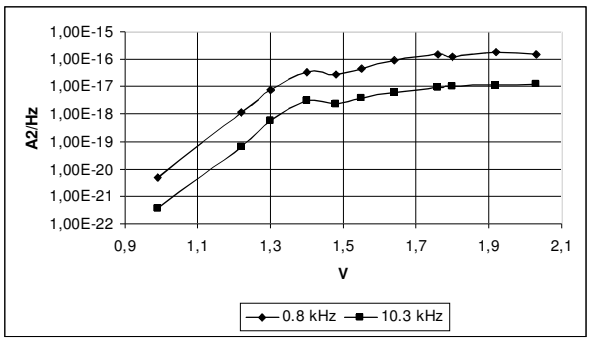


*b.*

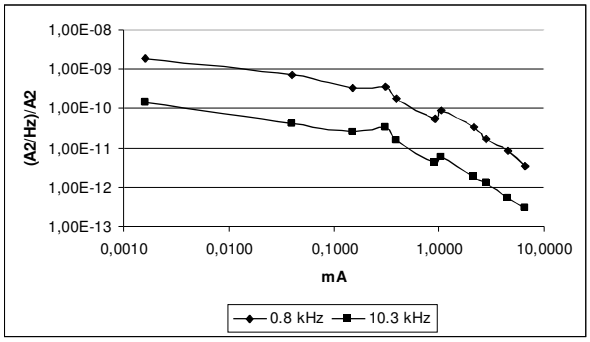


*a.* *c.*

*a.: The measured noise spectra at different biases; b.: the current noise in the function of bias voltage at two frequencies; c.: the normalised current noise in the function of the mean current.*

2. The **lead sulphide** has been used for a long time as infrared detector. Its spectral response extends to about 2.5 μm at room temperature. It exhibit excellent performance already at room temperature, and of course even better when cooled down. The main handicap of this material is its sensitivity to blue/ultraviolet light. Such exposures result in degradation: the dark conductivity will increase and subsequently the light/dark conductivity ratio decrease. We have followed the degradation process by the measurement of the low-frequency noise.

The PbS layers have been fabricated by the chemical deposition method onto glass substrates. The carefully cleaned glass was placed vertically in the aqueous solution at room temperature, for 10…25 minutes. The ohmic contacts were made by evaporation of Cr-Au contacts. The samples were mounted onto TO 5 transistor cases, the contact pads were bonded by thermocompressed gold wires. The sheet resistances of the layers were about 0.5…1 MΩsquare. The low-frequency (10Hz…20 kHz) noise characteristics were measured at different biases [152]. The forced degradation was produced by exposing the device to ultraviolet light. The noise spectra show 1/f type frequency decay. After the UV illumination the resistance of the samples decreased, however the noise characteristics were relatively unchanged. This behaviour is interpreted by the assumption that the noise arises from surface effects, while the resistance depends on the bulk properties.

### *Research and development of custom wavelength IR sources and detectors*

(in cooperation with the Ricola Ltd., Finland)

**V. Rakovics,** J. Balázs, S. Püspöki I. Réti, A. Tóth, Ms. Varga Ferencné, K. Vörös Veresné

***Aim and achievements:***

Portable IR spectrometers need efficient IR LEDs emitting in the 1000-1700 nm wavelength range.

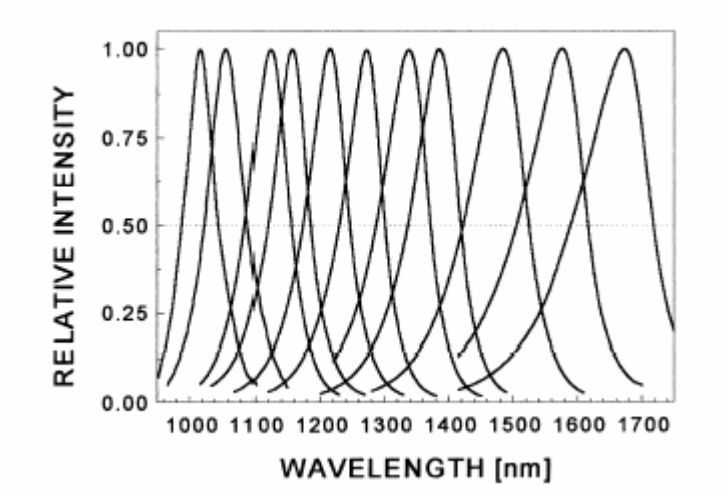


*Emission spectra of the 11 different type LEDs covering completely the 1000–1700 nm wavelength range*

The peak wavelength InGaAsP/InP double heterostructure LEDs can be tuned by the composition of quaternary InGaAsP. The 1000-1700 wavelength range was completely covered by 11 IR LEDs developed in MFA. LPE technology was used, for the growth of the LEDs.

New surface emitting LED construction was developed for IR spectrometer used for alcohol measurements. These types of LEDs have narrow beam angle and very high brightness.

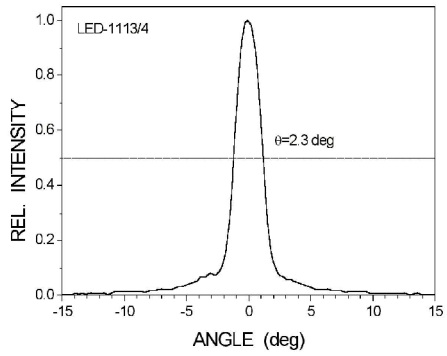


*Intensity distribution of narrow angle InGaAsP/InP LEDs*

Arrays of InGaAsP/InP single mode junction defined buried stripe heterostructure laser were grown on multi-channelled InP substrate by single-step liquid phase epitaxy [130]. The buried double heterostructure and the lateral current confining structure were formed in the same growth process. InGaAsP layer growth is dominated by the preferred orientation, with (1 0 0) growth favoured over other directions. As a result of low temperature single-step growth, the device yield is high. These laser arrays are characterised by output power close to 0.6W; high quantum efficiency, symmetrical far-field patterns and excellent linearity of the light–current curve. Stable single transverse mode operation obtained up to 600 mW emitted power.

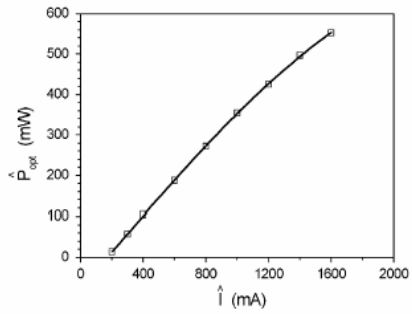


*Pulse light-current characteristics of the five element laser array.*

Portable IR spectrometers contain a linear array of LEDs or detectors and a fixed monochromator. We developed a linear array of PbS photoconductors [152]. The detector array can be used up to 3000 nm and have 14 active elements. Such wide spectral sensitivity is important for food spectroscopy and for some important medical applications (noninvasive glucose and urea measurement).

## Semiconductor Characterisation Laboratory (G. Battistig)

### *Thin film effects in semiconductor structures (OTKA T035272)*

**Z. J. Horváth**; M. Ádám, L. Dobos, B. Pődör, V. Rakovics, I. Szabó

Al, Au, Al/Ti, and Au/Ti contacts were prepared on n-GaN and annealed up to 900 ºC. The structure and morphology were studied by cross-sectional transmission and scanning electron microscopy and the electrical behaviour by current-voltage measurements. It was obtained that annealing yielded interdiffusion, lateral diffusion along the surface, alloying and bowling up of the metal layers. The electrical characteristics indicated that the upper metal layer in the Al/Ti and Au/Ti contacts diffused in and/or through the Ti layer even during deposition. A Schottky barrier height of 1.07 eV was obtained for Au metallisation. This value is closed to the Schottky limit of 1.00 eV indicating a low interface state density in the studied Au/n-GaN contacts. The main characteristics of electrical behaviour are summarised in Table 1.

*Table 1: The room temperature current-voltage behaviour and the estimated Schottky barrier height of Al/n-GaN contacts as a function of annealing temperature*

| Annealing temperature | Contact metal | | | |
|---|---|---|---|---|
| | Al | Al/Ti | Au | Au/Ti |
| As deposited | Rectifying, $\phi_b$<0.23 eV | Rectifying, $\phi_b$=0.38 eV | Rectifying, $\phi_b$=1.07 eV | Rectifying, $\phi_b$=0.49 eV |
| 300 ºC | Linear*, $\phi_b$<0.23 eV | Linear*, $\phi_b$<0.35 eV | Rectifying, $\phi_b$=0.93 eV | Rectifying, $\phi_b$=0.50 eV |
| 400 ºC | Linear*, $\phi_b$<0.23 eV | Linear*, $\phi_b$<0.35 eV | Rectifying, $\phi_b$=0.66 eV | Rectifying, $\phi_b$=0.44 eV |
| 700 ºC | Rectifying, $\phi_b$=0.27 eV | Linear*, $\phi_b$<0.35 eV | Rectifying, $\phi_b$=0.56 eV | Rectifying, $\phi_b$=0.43 eV |
| 900 ºC | No reliable measurement | No reliable measurement | No reliable measurement | Linear*, $\phi_b$<0.36 eV |

*Up to a current density level of 2 $Amm^{-2}$.

### *Studies of implantation and oxidation properties of SiC (OTKA T032029)*

**E. Szilágyi,** G. Battistig, N. Q. Khánh, P. Petrik, Z. Zolnai

The oxidation kinetics of 4H SiC on both the carbon- and the silicon-terminated surfaces were determined. The oxidation behaviours were compared to that obtained on the implantation amorphised SiC surface. It was demonstrated that oxidation kinetics increases on the Si-terminated side but slows down on the C-terminated surface. The kinetics obtained on implantation amorphised SiC resembles very much to that on the non-polar (11-20) SiC surface [158].

The lattice damage created by implantation of Al ions into single crystalline 4H-SiC has been analyzed using a combination of Rutherford Backscattering Spectrometry combined with channelling (RBS+C), Spectroscopic Ellipsometry (SE) and high resolution Transmission Electron Microscopy (XTEM) in a co-operation with Centro Nacional de Aceleradores, Seville, Spain. [12, 98, 116] After medium dose Al implantation (150 keV, $2\times10^{15}$ $cm^{-2}$) and high temperature annealing (1100 ºC, 1h, $N_2$) RBS+C showed, that highly damaged, amorphised layer remained at the surface. However SE demonstrated, that recrystallisation occurred, in the whole implanted region. Finally XTEM

proved, that solid phase epitaxy takes place during the high temperature treatment. Recrystallisation starts from the bulk, non-damaged region as well as from the less damaged very surface region. However recrystallisation does not follow everywhere the original crystal structure, grains with different polytypes and slightly different orientations are formed. RBS+C senses the crystal structure under a rather large area, the diameter of the used beam-spot is in the range of 0.5 mm. SE investigates the material also on a macroscopic surface but it senses the average refractive index of the material, a physical parameter what depends highly on the structure of the matter. The results obtained help to understand the physical processes taking place during ion implantation and annealing processes.

### *Theoretical Investigation of Point Defects and the Elementary Steps of Oxidation at the SiC/SiO$_2$ Interface (DFG-MTA bilateral project No. 112)*

**Z. Hajnal,** Á. Gali, P. Deák

Using a three-stage simulation framework – approximate DFTB for identification of possible defect configurations, DFT-LDA for precise formation energies, and hybrid DFT functionals with exact Hartree-Fock exchange for accurate defect levels – we study the (0001) interface of 4H-SiC and $SiO_2$. Our 2D slab model consists of a complete 4x4 layer of Si-terminated 4H-SiC with a double layer of $SiO_4$ tetrahedra on top. The upper and lower faces of the slab are saturated by H atoms. The structure has been constructed so, that it contains no dangling bonds, and no (or minimal) local stress. The energetics of various and Si-, O-, and C-defects as well as their complexes was determined using this 204 atom model, and supercells of bulk Si and $SiO_2$ (α-quartz). Assuming the oxidation of SiC proceeding in thermal equilibrium, the relative energies of reaction products can be used to draw possible reaction pathways of the system for $O_2$ addition and CO removal. Fig. 1. shows the resulting map with the energies of different resulting defect structures, and the final reaction equations of different paths.

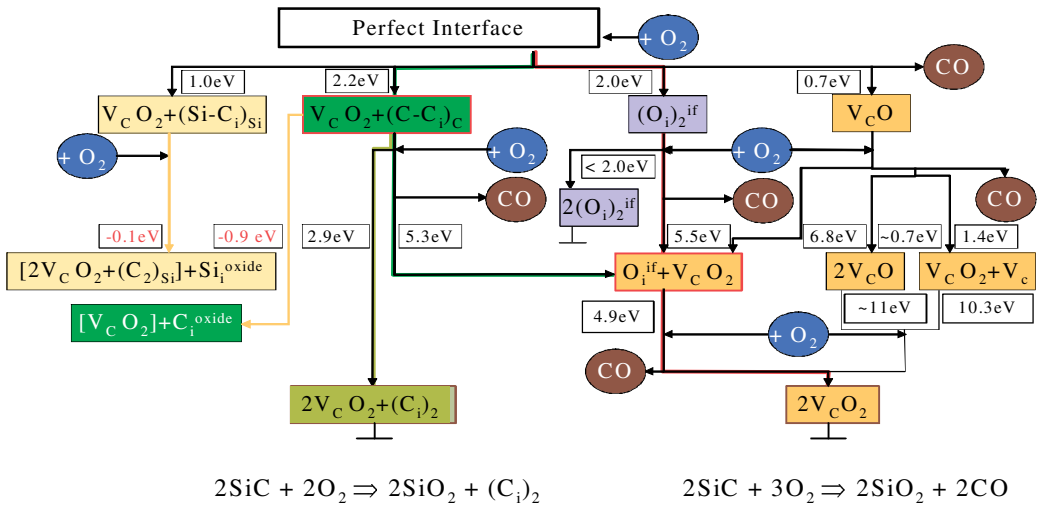


*Fig. 1: Reaction pathways related to the oxidation of SiC at the SiC/SiO$_2$ interface.*

### *Physics and Technology of Elemental, Alloy and Compound Semiconductor Nanocrystals - Materials and Devices, SEMINANO (EU FP6 No. 505285)*

**Z. J. Horváth,** M. Ádám, J. Balázs, P. Basa, L. Dobos, L. Dózsa, T. Lohner, G. Molnár, P. Petrik, P. Szöllõsi

Dielectric layers with embedded semiconductor nanocrystals are studied in order to overcome difficulties of non-volatile memory devices connected with technology scale-down, and to develop Si-based LEDs. One of the methods used for creating Si nanocrystals in $SiO_x$, is the high temperature annealing of these films containing excess Si. In our work the effect of high temperature annealing was studied on the composition, homogeneity, microstructure, and thickness of Si-rich $SiN_x$ layers by spectroscopic ellipsometry and cross-sectional transmission microscopy, and on their electrical behaviour by current-voltage, capacitance-voltage, conductivity-voltage, and memory hysteresis measurements.

The $SiN_x$ layers were deposited by low pressure chemical vapour deposition (LPCVD) at 800 ºC or 830 ºC and 0.35 mbar using $SiH_2Cl_2$ and $NH_3$. The average deposition rate was 3.5 nm/min. Three different layers were prepared on Si wafers with $SiH_2Cl_2$ to $NH_3$ ratio of 4:1, 3:1 or 1:4 which yielded different composition of $SiN_x$ layers with excess Si content of 6.9 %, 4.7 %, 0.2 %, respectively, as obtained by spectroscopic ellipsometry. Than the samples were cut for parts with an area of about 1 $cm^2$. Different parts of the wafers were annealed in forming gas in the temperature range of 800-1100 ºC for 1 hour. For electrical measurements Al capacitors were formed by evaporation and photolitography.

It has been obtained by cross-sectional transmission microscopy that the layers remained amorphous after each annealing step. No systematic dependence of the layer thickness has been obtained on the annealing conditions. It is likely, that the small scatter of layer thickness obtained by ellipsometry and XTEM measurements, is due to the lateral inhomogeneity of the original as-deposited samples. However, it has been obtained by spectroscopic ellipsometry that the Si content of the layers decreased slightly with increasing annealing temperature.

The electrical behaviour were strongly affected by annealing. Systematic dependences of the flat-band voltage and the electrical conductivity have been obtained up to annealing temperature of 1000 ºC, but annealing at 1100 ºC have degraded the layers. Consequently, the memory behaviour also have depended on annealing.

### *Front-End Models for Silicon Future Technology – FRENDTECH, (IST Project 2000-30129, 2002-2004)*

**G. Battistig,** T. Lohner, M. Ádám, P. Petrik, P. Deák, K. Kamarás

The activation rate of shallow boron implants can be maximised by optimizing the subsequent annealing, which has to dissolve the boron-interstitial clusters (BIC) formed during implantation. This requires the knowledge of the formation energies of the dominant BICs. Previous theoretical analysis at *ab initio* level has found a large number of possible complexes and predicted their formation energies with an error bar of about 1 eV. Regarding the number of BICs (15-20) this error introduces uncertainties in kinetic simulations. Therefore, it is desirable to identify the dominant BICs by spectroscopic methods. For that purpose, the measurable properties of all possible BICs have to be calculated *a priori* with high precision.

Therefore, sophisticated *ab initio* calculations have been carried out systematically on a large-scale, to establish a data base for the vibration spectra (normal mode frequencies)

and electronic structure (one-electron level positions in the gap) for all BICs. After the necessary convergence tests, the silicon crystal, containing the BICs, was simulated by an appropriate supercell model. The total energy and the equilibrium geometry were calculated using density functional theory (DFT) and norm conserving pseudopotentials. The vibration spectra have been determined in the harmonic approximation for all possible isotope composition, using generalised gradient approximation (GGA) and numerical atomic orbitals. The electronic structure was calculated with an optimised hybrid functional and Gaussian orbitals. As a by-product, some long standing controversies in the interpretation of experimental results on the simplest boron complexes could be solved.

### *Ion implantation of SiC using in channelling direction*

**N. Q. Khanh,** T. Lohner, Z. Zolnai, A. Ster

500 keV $N^+$ implantation with different fluences and different orientations with respect to the <0001> crystallographic axis (the c-axis) of 6H-SiC has been performed using the EG-2R Van de Graaff accelerator. The implantation-induced damage distributions in both the Si and C sublattices were measured by 3.55 MeV $^4He^+$ backscattering spectrometry/channelling (BS/C) analysis. For an adequate energy-depth conversion in BS/C spectra, the electronic stopping power of the analyzing He ions along the c-axis of SiC has been determined. The damage distributions, provided by BS/C were compared to the results of Crystal-TRIM computer simulations. We have found that the dependence of the shape of damage distributions in function of the tilt angle between the N ions and the c-axis of 6H-SiC can be well reconstructed at relatively low fluences. Contrary, for highly damaged layers a large discrepancy has been observed between experiment and simulation, that can be attributed to secondary damage formation processes, dominating the amorphisation of SiC in the high-fluence region [176, 177, 178]. The results were published at the 5th European Conference on Silicon Carbide and Related Materials (ECSCRM 2004, Aug 31 - Sept 4, 2004, Bologna, Italy).

### *Nucleation of SiC nanocrystals at the Si/$SiO_2$ interface: effect of the interface properties*

**G. Battistig,** A. Pongrácz, A. L. Tóth, Z. Makkai, Z. Hajnal

Significant work has been recently devoted to the growth of Si nanocrystals (NCs) because of their possible application for non-volatile memory devices and Si based LEDs. Our group have proposed a simple method for SiC NCs growth at the Si side of the Si/$SiO_2$ interface during annealing in CO atmosphere. The size and shape of the crystallites are typically uniform. As the NCs grow epitaxially and void-free on the Si substrate this structure might be used as seed crystals at the epitaxial growth of SiC on Si.
Further oxidation of the Si/$SiO_2$ structure containing SiC grains produce a system, where the NCs sit in the oxide, which is suitable for flash memory applications. The nanometre sized SiC grains could have further importance in the optoelectronic applications.
Additional investigations are necessary to understand the nucleation and growth mechanism of the SiC NCs in order to control the nucleation density and grain size. Recently we examined the effect of the Si/$SiO_2$ interface properties on nucleation process.
(100), (110) and (111) Si substrates covered with 100 nm thick thermally grown $SiO_2$ layer were heat treated in CO containing ambient for several hours. Low voltage scanning electron microscopy (SEM) was used to obtain information about the microstruc-

ture of the system. Cross sectional and plan view images have been taken from the samples (Fig. 2.).

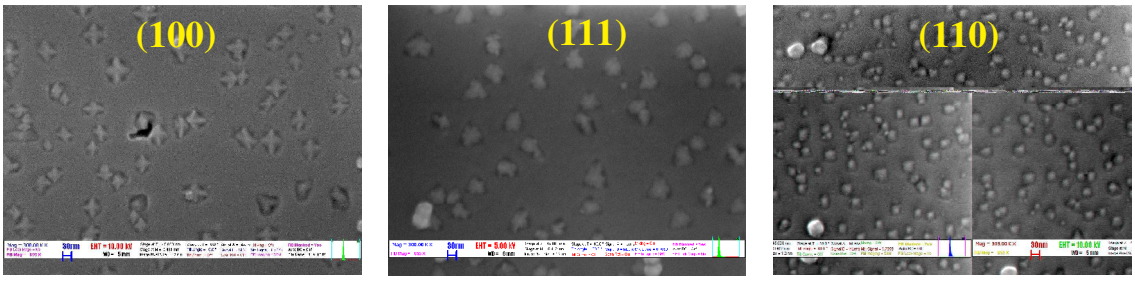


*Fig. 2: SiC nanocrystals grown on (100), (110) and (111) Si substrates*

Size, morphology and nucleation density of the nanocrystals have been found to depend strongly on the orientation of the substrates. Comparing the (110) plane with the other crystal planes the typical grain size is smaller and the nucleation density is one range higher.